High-resolution three-dimensional imaging of biofilm development using optical coherence tomography

Chuanwu Xi*
University of Illinois at Urbana-Champaign
Department of Civil and Environmental Engineering
Biophotonics Imaging Laboratory
Beckman Institute for Advanced Science and Technology
Urbana, Illinois 61801
E-mail: cxi@umich.edu

Daniel Marks
Simon Schlachter
Wei Luo
University of Illinois at Urbana-Champaign
Biophotonics Imaging Laboratory
Beckman Institute for Advanced Science and Technology
Urbana, Illinois 61801

Stephen A. Boppart
University of Illinois at Urbana-Champaign
Biophotonics Imaging Laboratory
Department of Electrical and Computer Engineering
Department of Bioengineering
Department of Internal Medicine
Beckman Institute for Advanced Science and Technology
Urbana, Illinois 61801
E-mail: boppart@uiuc.edu

Abstract. We describe the use of optical coherence tomography (OCT) for high-resolution, real-time imaging of three-dimensional structure and development of a *Pseudomonas aeruginosa* biofilm in a standard capillary flow-cell model. As the penetration depth of OCT can reach several millimeters in scattering samples, we are able to observe complete biofilm development on all surfaces of a 1 mm $\times$1 mm flow-cell. We find that biofilm growing at the bottom of the tube has more structural features including voids, outward projections, and microcolonies while the biofilm growing on the top of the tube is relatively flat and contains less structural features. Volume-rendered reconstructions of cross-sectional OCT images also reveal three-dimensional structural information. These three-dimensional OCT images are visually similar to biofilm images obtained with confocal laser scanning microscopy, but are obtained at greater depths. Based on the imaging capabilities of OCT and the biofilm imaging data obtained, OCT has potential to be used as a non-invasive, label-free, real-time, *in-situ* and/or *in-vivo* imaging modality for biofilm characterization. [DOI: 10.1117/1.2209962]

Keywords: biofilm structure; optical coherence tomography; imaging; development.

Paper 05316R received Oct. 20, 2005; revised manuscript received Jan. 4, 2006; accepted for publication Jan. 9, 2006; published online Jun. 26, 2006.

1 Introduction

Micro-organisms (bacteria, fungi, and/or protozoa, with associated bacteriophages and other viruses) can grow collectively in adhesive polymers [mainly extracellular polysaccharides (EPS)] on biologic or nonbiologic surfaces to form biofilms. Biofilms are ubiquitous in natural and industrial environments, and it is now thought that biofilms are the primary habitat for many micro-organisms, as biofilm can protect microbes from harsh environments such as the presence of antibiotics and biocides.[1–3] Biofilms have been associated with a wide range of problems both in industry and medicine, as it is very difficult to eradicate them with common practice. According to the National Institutes of Health, biofilms account for more than 80% of microbial infections in the body.[4] Biofilms can virtually colonize any indwelling device (catheters, artificial joints, and contact lenses) and different tissues (oral soft tissues, teeth, middle ear, gastrointestinal tract, urogenital tract, airway/lung tissue, etc.).[5–8] Biofilms colonized on devices are the sources of most medical device-related infections.[9] Currently, there are few, if any, effective strategies to impede the process of biofilm colonization of these devices. The use of a high-resolution, 3-D imaging modality offers the potential to improve our visualization and understanding of the complex dynamics within biofilms.

Biofilms in earlier literature were shown to be a homogenous distribution of cells in a uniform exopolysaccharide matrix that lacks heterogeneity in structure.[10] The application of optical imaging techniques, especially confocal scanning laser microscopy (CSLM), radically altered the perception of biofilm structure and function.[11] Most biofilms have been found to exhibit some level of heterogeneity in structure with a variable distribution of cells and cellular aggregates, variable density of extracellular polymers, and void spaces or water channels.[1,12] These heterogeneous features appear to be common to most biofilms, as they were not only found in mixed-cultured biofilms but also found in monospecies biofilms.[1,13] The biofilm structure can be affected by numerous environmental parameters and may have a direct relationship with biofilm function. It was suggested that the structural diversity actually reflects the adaptation of unicellular organisms to a diverse range of physical, chemical, and communal circumstances on surfaces.[1]

A number of optical and nonoptical imaging techniques have been developed previously for use in the study of biofilm structure and development. These techniques include, but are not limited to, light microscopy,[10,14] electron microscopy,[15] CSLM,[11,16] infrared spectroscopy,[17] reflectance spectroscopy,[16] optical fluorometry,[18,19] nuclear magnetic resonance imaging (NMRI),[20–24] atomic force microscopy (AFM),[25] and photoacoustic spectroscopy.[26] The study of biofilms using these imaging techniques has revealed many fea-

*Current affiliation: The Univ. of Michigan, School of Public Health, Dept. of Environmental Health Sciences, Ann Arbor, MI 48109.

1083-3668/2006/11(3)/034001/6/$22.00 © 2006 SPIE

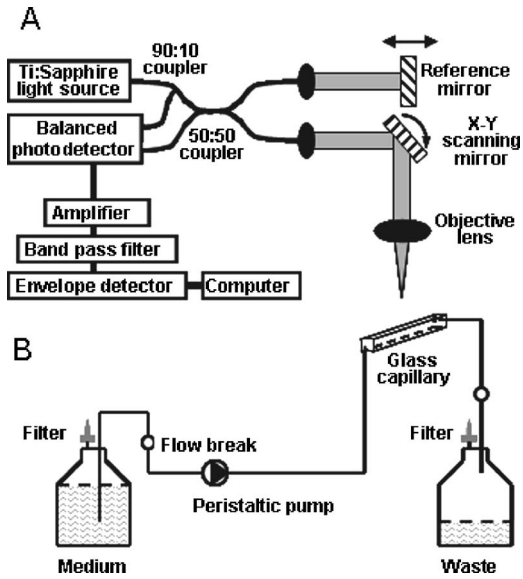

Fig. 1 Experimental set-up. (a) Schematic diagram of the OCT imaging system, and (b) biofilm reactor system. The cross sectional dimension of the glass flow-cell tube is 1×1 mm.

tures of biofilms and furthered our understanding of biofilm structure and function. However, there are limitations associated with each technique. For example, sample preparation for electron microscopy will alter the original structure of biofilms. CSLM is very widely used for biofilm research; however, cell labeling requirements limit its use for study of natural biofilm *in vivo*, and shallow imaging penetration limits its application in the study of very thick biofilms. NMRI can be used to image biofilm structure and flow profiles in biofilms; however, low image resolution and long acquisition times for images limit its application in biofilm monitoring in real time.

Optical coherence tomography (OCT) is an emerging high-resolution medical and biological imaging technology[27–31] that can perform optical ranging of biological and nonbiological structures in a manner similar to ultrasound [Fig. 1(a)]. Because OCT uses the shorter wavelengths of near-infrared light rather than sound, imaging resolution can be 10 to 100 times higher. Near-infrared wavelengths are used in OCT imaging to increase imaging penetration through highly scattering structures. It is possible to image depths of several centimeters through transparent structures and of a few millimeters in highly scattering tissue. We report the first use of OCT to image biofilms, specifically a *Pseudomonas aeruginosa* biofilm developed in a capillary flow cell, which is representative of a wide range of scenarios where biofilms develop. This particular bacteria species was chosen for this study, since it is a virulent pathogen commonly found to colonize on medical catheters, tubing, and devices in clinical settings, and its biofilm structures developed under different conditions have been reported previously.[11,32–36] We demonstrate that OCT techniques have the potential for noninvasive, label-free, real-time and *in-situ* and/or *in-vivo* characterization of biofilm structure and function.

2 Materials and Methods

2.1 *Bacterial Strains, Culture Conditions, and Biofilm Development*

Pseudomonas aeruginosa PAO1 was used throughout this study. To visualize the same biofilm growth with OCT and CSLM, the strain PAO1 was transformed with a plasmid pMP4655 carrying an *egfp* gene.[37] Green fluorescent protein (GFP) was expressed constitutively. Strains were routinely cultured on Trypticase soy agar (Becton Dickinson, Sparks, MD), and when appropriate, tetracycline was added (final concentration of 20 μg/ml). A dilute broth medium (Trypticase soy broth [TSB], pH 6.8) at a concentration of 3 g per liter (dTSB) was used for the flow system to grow biofilms.

Biofilms were cultivated in a single-channel flow cell (1×1 mm, Biosurface Technologies, Bozeman, Montana) supplied with diluted TSB at a flow rate of 0.3 ml/min for 72 h using a L/V Variable Speed Digital Drive Pump system (Cole Parmer, Vernon Hills, Illinois) [Fig. 1(b)]. Procedures for growing biofilms in the flow cell were as described previously.[38,39]

Pseudomonas aeruginosa PAO1 was also inoculated into an optical polystyrene (OPS) cuvette ($10 \times 10 \times 45$ mm, VWR, Batavia, Illinois) filled with one third of volume of TSB and incubated at 30 °C with shaking at 100 rpm for 72 h. Biofilms developed on the inner wall of the cuvette, and the interface of air and media were imaged with OCT.

2.2 *Optical Coherence Tomography*

The OCT system consisted of galvanometer-scanned mirrors for the delay mechanism and the transverse scanning. The optical source was a mode-locked Ti-sapphire laser (Kapteyn-Murnane Laboratories, Incorporated, Boulder, Colorado) centered at 800 nm with an output of approximately 100-nm bandwidth (2.8-μm axial resolution). The 1.3-mm-diameter beam was incident on the back aperture of a 20-mm focal length achromatic lens, giving a free-space numerical aperture of 0.065. The light was focused to a 15-μm spot size (transverse resolution), with a corresponding confocal parameter of approximately 442 μm. The focus was placed approximately 300 μm above the bottom surface of the flow-cell tube to optimize visualization of features at both the bottom and top surfaces. Image acquisition rates were 15 to 30 s, depending on image size, and could be considerably faster (4 to 32 fps) using more sophisticated delay-line scanning mechanisms[40,41] or spectral-domain OCT detection.[42–44] Biofilms growing in the flow cell were continuously imaged every 4 or 8 h for up to 72 h.

2.3 *Fluorescence Microscopy and Confocal Scanning Laser Microscopy*

Fluorescence microscopy and CSLM (Model DM-IRE, Leica Microsystems, Bensheim, Germany) were used to acquire fluorescent images of *P. aeruginosa* growing on the surface at the bottom of the glass flow-cell tube. A wavelength of 488 nm was used to excite the GFP, and the 514-nm emission wavelength was detected in the epidirection. Samples were imaged in the sequential mode with 63× and 20× objectives.

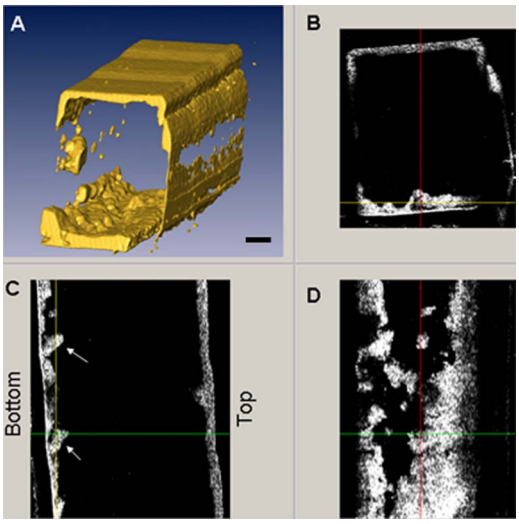

Fig. 2 OCT imaging of a 3-day *P. aerogenosa* biofilm in the glass capillary of a biofilm flow cell. The dimension of the tube is 1 ×1 mm and the length of the visualized biofilm is 2 mm. (a) Volume-rendered 3-D reconstruction of the biofilm from a series of 128 cross sectional images. (b) Cross sectional OCT image of the biofilm shown in (a). (c) Vertical section of biofilm shown in (a), along the length of the tube. Bottom and top of the tube are indicated. Arrows indicate projections or "mushrooms" in the biofilm at the bottom. (d) Horizontal section of biofilm along the bottom. Scale bar represents 200 μm.

2.4 *Image Analysis*

3-D volumetric CSLM images were reconstructed from a series of 28 horizontal-sectional images spaced at 1-μm separation using commercial software (Slicer Dicer, Pixotec, LLC, Renton, Washington). 3-D volumetric OCT images were reconstructed from a series of 128 cross sectional images spaced at 15.5-μm separation using commercial software (Slicer Dicer, Pixotec, LLC, Renton, Washington, or Amira, Zuse Institute, Berlin, Germany). 2-D cross sectional OCT images along the *Y* and *Z* axes were also obtained with the same software.

3 Results

OCT, as an emerging high-resolution imaging technology, has been widely applied in medical and biological research. To test the potential of OCT in the study of biofilm structure and function, we imaged a *Pseudomonas aeruginosa* PAO1 biofilm using a time-domain OCT system similar to the one used to image structure and fluid flow in microfluidic mixers.[45]

A 3-D image of the biofilm (72 h after inoculation) developed on the inner surfaces of glass flow cell was reconstructed and volume rendered using commercial software (Amira, Zuse Institute, Berlin, Germany) [Fig. 2(a)], which clearly shows a complete biofilm developed in the tube. More detailed visualization of structure inside the biofilm can be obtained from 2-D sections of 3-D dataset at different planes [Figs. 2(b)–2(d)]. Figure 2(b) shows a cross sectional OCT image of the biofilm. Cell aggregates separated by interstitial voids and water channels are clearly seen. The biofilm on the top of the tube is flatter than the biofilm at the bottom. More projections or "mushrooms" of bacterial aggregates are visible on the surface at the bottom of the tube than on the top.

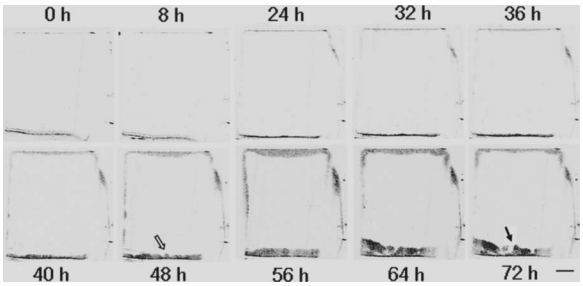

Fig. 3 OCT imaging of biofilm growth. Sequential 2-D OCT images of *P. aerogenosa* biofilm growth dynamics in the glass flow cell. Imaging times are indicated above or below the corresponding figure. Biofilm growth on the bottom of the flow cell includes multiple projections (indicated with open arrow) and voids (indicated with solid black arrows). Scale bar represents 200 μm.

Biofilm growth dynamics were also monitored (Fig. 3). Twenty-four hours after inoculation, signals indicating cell growth on the surface at the bottom of the glass capillary can be observed, and more cells accumulate on the surfaces with longer incubation time. Microcolonies are clearly seen two days after inoculation. Biofilm structural features, including interstitial voids, water channels, and "mushrooms" of bacterial aggregates, are visible by three days after inoculation. On the top of the glass tube, OCT signals indicate less biofilm growth, compared to that at the bottom, and the biofilm surface is relatively flatter.

We also developed a *P. aeruginosa* biofilm in a cuvette (see materials and methods) and scanned a portion (2 ×2 mm) of the biofilm (Fig. 4). Different cell aggregates were observed embedded in the likely heterogeneous density of the extracellular polymer matrix. Voids (spaces) are clearly observed [Fig. 4(a)]. A reconstructed 3-D image registers a floating piece of biofilm as shown in Fig. 4(b).

For comparison, fluorescence microscopy (FM) and CSLM were used to image the early stages (0 to 48 h) of *P. aeruginosa* biofilm development at the bottom in these flow cells (Fig. 5). Detailed structures including initial sites of colonization and spreading growth patterns are evident from FM and CSLM. Structural features of *P. aeruginosa* biofilm development at the bottom revealed by CSLM and OCT are visually similar (Figs. 2 and 5).

4 Discussions

The biofilm structural data obtained from OCT are visually similar with data obtained from other imaging techniques. Mathematical interpretation of the data and optical property measurements of these biofilms obtained with OCT are currently underway and will provide additional information. More interestingly, we were able to completely image with high resolution the biofilms developed in the flow-cell tube to a depth of about 2 mm as a result of the OCT imaging depth. We were also able to scan large areas and 3-D volumes of biofilms with high resolution. These data clearly demonstrated that OCT is a novel and useful imaging technology to characterize biofilm development dynamics under different conditions.

The resolution of the OCT system used in this study was high (2.8-μm axial, 15-μm transverse). However, these reso-

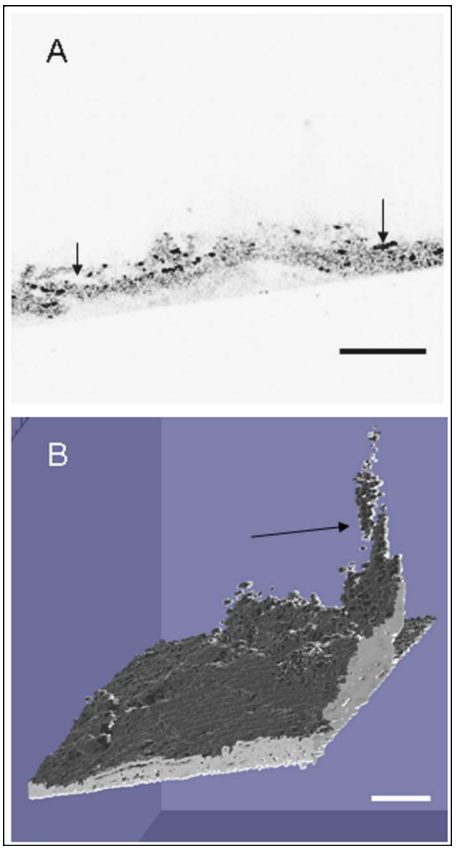

Fig. 4 OCT imaging of an interfacial biofilm. A 3-day *P. aeruginosa* biofilm developed at the interface of air and culturing media is shown. The area scanned is 2×2 mm. (a) cross sectional OCT image of the biofilm showing microbial cell aggregates and matrix. Arrows indicate cell aggregates (right) and voids (left). (b) 3-D reconstruction of the biofilm showing uneven surfaces and detachment of cell aggregates (indicated by arrow). Scale bars represent 400 μm.

lutions are not sufficient to image individual bacterial cells, which may limit OCT for the application in bacterial adhesion studies. FM and CSLM were used to image the earliest stages of biofilm development for comparison purposes (Fig. 5). Detailed structures shown with FM and CSLM imaging are evident, and structural features at later stages (48 h) revealed by CSLM and OCT look similar (Figs. 2 and 5). While FM and CSLM are able to identify single fluorescing bacteria and small microcolonies, imaging of biofilms using FM and CSLM requires that the microscope objective be in close proximity to the biofilm surface, and is typically limited in the depth of imaging penetration to less than one hundred microns. Submicron OCT imaging is feasible by incorporating ultrabroad-bandwidth titanium:sapphire lasers,[46,47] and the use of these sophisticated laser systems may enable OCT to study these earliest stages of biofilm development as well. Still, the resolutions afforded by the OCT system in this study and other state of the art systems enables the larger-scale imaging of microbial colonies, and the microstructure that develops in these biofilms. Further research is underway to expand the resolution capabilities of our OCT systems, including the use of optical coherence microscopy (OCM).

Implementing other OCT-related techniques will further improve the characterization of biofilm structure and function. Flow dynamics will have significant effects on biofilm structure and function. OCT is not only capable of imaging 3-D microstructures at micron-scale resolutions, but can also obtain velocity profiles at real-time acquisition rates in small lumens and vessels[48–51] in a manner analogous to laser-Doppler velocimetry or Doppler ultrasound. Doppler OCT has been used in our previous studies to visualize fluid flow velocity profiles in capillary tubes and microfluidic channels.[45] Doppler OCT imaging can be used to provide quantitative information on biofilm dynamics, flow velocities, and flow distributions during the formation of biofilms within catheters

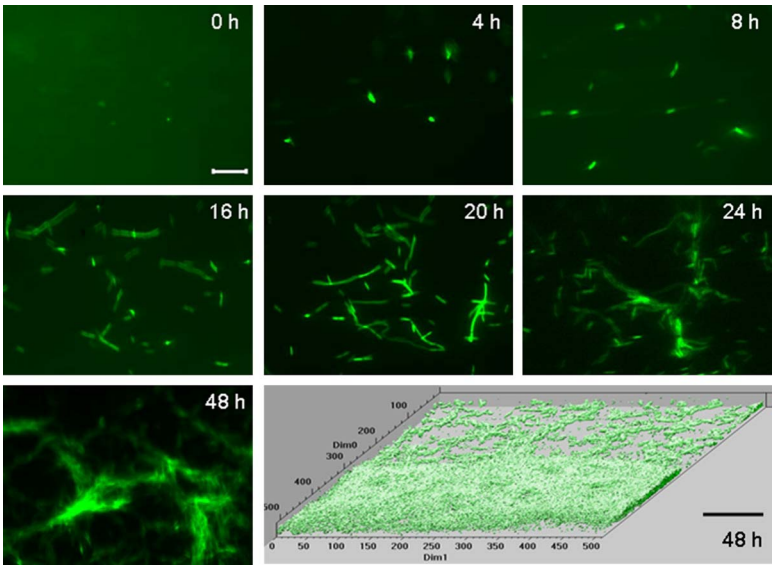

Fig. 5 Fluorescence microscopy and confocal scanning laser microscopy of biofilm growth. Early stages of biofilm growth are shown at the bottom of the glass flow-cell tube. Time sequence over the initial 48 h shows isolated GFP-labeled bacteria (at 4 h), which develop into microcolonies (8 h) and proliferate (16 to 48 h) to form a thin relatively smooth surface. The lower right image is a volume-rendered 3-D reconstruction of the biofilm from a series of 16 *en face* CLSM sections. Scale bar represents 10 μm in the fluorescence micrographs and 50 μm in the 3-D CSLM dataset.

or tubes. It may be necessary, however, to add certain scattering contrast agents such as lipids or proteins or inert nanoparticles for this purpose if the bacteria-laden fluids or nutrient-rich media lack sufficient optical scattering properties.

Substrates and nutrient heterogeneity in biofilms will often define biofilm structure and function. A technique called spectroscopic OCT or spectroscopic OCM (SOCT/SOCM)[52–54] enables high-resolution spatial localization of *spectroscopic* information from a sample, which can be used to identify and characterize certain chemicals, absorbers, and scatterers. We expect that spectroscopic OCT/OCM will enable the study of substrate gradients and consumption dynamics in biofilms, as well as enable the investigation of interaction dynamics between cells and substrates.

It is likely that OCT/OCM can differentiate cells and the polymer matrix in biofilms, as the scattering properties of cells and polymers differ. By setting a threshold of pixel intensity within the OCT images, it may be possible to differentiate cells and polymers so that biomass can be calculated from each image, as shown in Fig. 3. This research is currently under investigation. In addition, the acquisition rates of spectral-domain OCT now can reach 30 frames per second or greater, depending on image size, making it possible to acquire images of complete biofilm development in real time and compute bacterial growth in biofilms in 3-D volumes in real time. These quantitative data will be useful for mathematically modeling biofilm growth, as it will provide data of a complete biofilm rather than a portion of a biofilm.

OCT has been used to image both *in-situ* and *in-vivo* tissues and identify regions that suggest abnormalities that should be biopsied for histopathological examination.[55–57] OCT catheters have been developed for internal imaging of tubular lumens, and an intravascular OCT imaging system was recently developed for *in-vivo* intravascular imaging in humans.[58] We expect that catheter-based OCT systems will permit *in-situ* imaging and analysis of biofilms developing on medical tubing and hollow catheters such as endotrachial tubes, vascular-access catheters, and urinary catheters. This will enable the *in-vivo* characterization of biofilms developed in clinical and natural environments. Similar OCT imaging catheters will also permit visualization and investigation of tubing and pipeworks in industrial systems.

By fully employing these existing capabilities of OCT, there is a significant potential for OCT to be used as a noninvasive, label-free, real-time, *in-situ* and/or *in-vivo* imaging modality for biofilm characterization.

Acknowledgments

We thank, from the Beckman Institute for Advanced Science and Technology at the University of Illinois, Urbana-Champaign, Tyler Ralston for his technical assistance in acquiring OCT images, and Janet Sinn-Hanlon for her help with processing and rendering images. This work was supported in part by the National Institutes of Health (NIH) (1 R01 EB00108, S.A.B.). Additional information can be found at: http://biophotonics.uiuc.edu.

References

1. J. W. Costerton, Z. Lewandowski, D. E. Caldwell, D. R. Korber, and H. M. Lappin-Scott, "Microbial biofilms," *Annu. Rev. Microbiol.* **49**, 711–745 (1995).
2. L. Hall-Stoodley, J. W. Costerton, and P. Stoodley, "Bacterial biofilms: From the natural environment to infectious diseases," *Nat. Rev. Microbiol.* **2**, 95–108 (2004).
3. G. O'Toole, H. B. Kaplan, and R. Kolter, "Biofilm formation as microbial development," *Annu. Rev. Microbiol.* **54**, 49–79 (2000).
4. D. Davies, "Understanding biofilm resistance to antibacterial agents," *Nat. Rev. Drug Discovery* **2**(2), 114–122 (2003).
5. R. M. Donlan, "Biofilms: Microbial life on surfaces," *Emerg. Infect. Dis.* **8**, 881–890 (2002).
6. R. M. Donlan, "Biofilms and device-associated infections," *Emerg. Infect. Dis.* **7**, 277–281 (2001).
7. J. W. Costerton, P. S. Stewart, and E. P. Greenberg, "Bacterial biofilms: A common cause of persistent infections," *Science* **284**, 1318–1322 (1999).
8. C. A. Fux, J. W. Costerton, P. S. Stewart, and P. Stoodley, "Survival strategies of infectious biofilms," *Trends Microbiol.* **13**, 34–40 (2005).
9. B. W. Trautner, R. A. Hull, and R. O. Darouiche, "Prevention of catheter-associated urinary tract infection," *Curr. Opin. Infect. Dis.* **18**, 37–41 (2005).
10. R. Bakke and P. Q. Olsson, "Biofilm thickness measurements by light-microscopy," *J. Microbiol. Methods* **5**, 93–98 (1986).
11. J. R. Lawrence, D. R. Korber, B. D. Hoyle, J. W. Costerton, and D. E. Caldwell, "Optical sectioning of microbial biofilms," *J. Bacteriol.* **173**, 6558–6567 (1991).
12. M. E. Davey and A. O'Toole G, "Microbial biofilms: From ecology to molecular genetics," *Microbiol. Mol. Biol. Rev.* **64**, 847–867 (2000).
13. J. Wimpenny, W. Manz, and U. Szewzyk, "Heterogeneity in biofilms," *FEMS Microbiol. Rev.* **24**, 661–671 (2000).
14. R. Bakke, R. Kommedal, and S. Kalvenes, "Quantification of biofilm accumulation by an optical approach," *J. Microbiol. Methods* **44**, 13–26 (2001).
15. B. Nyvad and O. Fejerskov, "Assessing the stage of caries lesion activity on the basis of clinical and microbiological examination," *Community Dent. Oral Epidemiol.* **25**, 69–75 (1997).
16. M. Wiggli, A. Smallcombe, and R. Bachofen, "Reflectance spectroscopy and laser confocal microscopy as tools in an ecophysiological study of microbial mats in an alpine bod pond," *J. Microbiol. Methods* **36**, 239–240 (1999).
17. D. E. Nivens, J. Q. Chambers, T. R. Anderson, A. Tunlid, J. Smit, and D. C. White, "Monitoring microbial adhesion and biofilm formation by attenuated total reflection Fourier-transform infrared-spectroscopy," *J. Microbiol. Methods* **17**, 199–213 (1993).
18. H. Beyenal, C. Yakymyshyn, J. Hyungnak, C. C. Davis, and Z. Lewandowski, "An optical microsensor to measure fluorescent light intensity in biofilms," *J. Microbiol. Methods* **58**, 367–374 (2004).
19. R. Thar, M. Kuhl, and G. Holst, "Fiber-optic fluorometer for microscale mapping of photosynthetic pigments in microbial communities," *Appl. Environ. Microbiol.* **67**, 2823–2828 (2001).
20. B. Manz, F. Volke, D. Goll, and H. Horn, "Measuring local flow velocities and biofilm structure in biofilm systems with magnetic resonance imaging (MRI)," *Biotechnol. Bioeng.* **84**, 424–432 (2003).
21. M. Paterson-Beedle, K. P. Nott, L. E. Macaskie, and L. D. Hall, "Study of biofilm within a packed-bed reactor by three-dimensional magnetic resonance imaging," *Methods Enzymol.* **337**, 285–305 (2001).
22. J. D. Seymour, S. L. Codd, E. L. Gjersing, and P. S. Stewart, "Magnetic resonance microscopy of biofilm structure and impact on transport in a capillary bioreactor," *J. Magn. Reson.* **167**, 322–327 (2004).
23. Z. Lewandowske, S. A. Altobelli, and E. Fukushima, "NMR and miciroelectrode studies of hydrodynamics and kinetics in biofilms," *Biotechnol. Prog.* **9**, 40–45 (1993).
24. Z. Lewandowski, S. A. Altobelli, P. D. Majors, and E. Fukushima, "NMR imaging of hydrodynamics near microbially colonized surfaces," *Water Sci. Technol.* **26**, 577–584 (1992).
25. R. J. th Emerson and T. A. Camesano, "Nanoscale investigation of pathogenic microbial adhesion to a biomaterial," *Appl. Environ. Microbiol.* **70**, 6012–6022 (2004).
26. T. Schmid, C. Helmbrecht, U. Panne, C. Haisch, and R. Niessner, "Process analysis of biofilms by photoacoustic spectroscopy," *Anal. Bioanal. Chem.* **375**, 1124–1129 (2003).
27. B. E. Bouma and G. J. Tearney, *Handbook of Optical Coherence Tomography*, Marcel Dekker, New York, (2001).
28. D. Huang, E. A. Swanson, C. P. Lin, J. S. Schuman, W. G. Stinson,

W. Chang, M. R. Hee, T. Flotte, K. Gregory, C. A. Puliafito, and J. G. Fujimoto, "Optical coherence tomography," *Science* **254**, 1178–1181 (1991).
29. G. J. Tearney, M. E. Brezinski, B. E. Bouma, S. A. Boppart, C. Pitris, J. F. Southern, and J. G. Fujimoto, "*In vivo* endoscopic optical biopsy with optical coherence tomography," *Science* **276**, 2037–2039 (1997).
30. S. A. Boppart, G. J. Tearney, B. E. Bouma, J. F. Southern, M. E. Brezinski, and J. G. Fujimoto, "Noninvasive assessment of the developing *Xenopus* cardiovascular system using optical coherence tomography," *Proc. Natl. Acad. Sci. U.S.A.* **94**, 4256–4261 (1997).
31. S. A. Boppart, B. E. Bouma, C. Pitris, J. F. Southern, M. E. Brezinski, and J. G. Fujimoto, "*In vivo* cellular optical coherence tomography imaging," *Nat. Med.* **4**, 861–865 (1998).
32. A. Heydorn, A. T. Nielsen, M. Hentzer, C. Sternberg, M. Givskov, B. K. Ersboll, and S. Molin, "Quantification of biofilm structures by the novel computer program COMSTAT," *Microbiology* **146**(Pt 10), 2395–2407 (2000).
33. S. Takenaka, M. Iwaku, and E. Hoshino, "Artificial *Pseudomonas aeruginosa* biofilms and confocal laser scanning microscopic analysis," *J. Infect. Chemother.* **7**(2), 87–93 (2001).
34. R. C. Hunter and T. J. Beveridge, "High-resolution visualization of *Pseudomonas aeruginosa* PAO1 biofilms by freeze-substitution transmission electron microscopy," *J. Bacteriol.* **187**(22), 7619–7630 (2005).
35. K. Sauer, A. K. Camper, G. D. Ehrlich, J. W. Costerton, and D. G. Davies, "*Pseudomonas aeruginosa* displays multiple phenotypes during development as a biofilm," *J. Bacteriol.* **184**(4), 1140–1154 (2002).
36. P. Stoodley, Z. Lewandowski, J. D. Boyle, and H. M. Lappin-Scott, "Structural deformation of bacterial biofilms caused by short-term fluctuations in fluid shear: An *in situ* investigation of biofilm rheology," *Biotechnol. Bioeng.* **65**(1), 83–92 (1999).
37. G. V. Bloemberg, A. H. Wijfjes, G. E. Lamers, N. Stuurman, and B. J. Lugtenberg, "Simultaneous imaging of *Pseudomonas fluorescence* WCS365 populations expressing three different autofluorescent proteins in the rhizosphere: New perspectives for studying microbial communities," *Mol. Plant-Microbe Interact.* **13**, 1170–1176 (2000).
38. R. C. Hunter and T. J. Beveridge, "Application of a pH-sensitive fluoroprobe (C-SNARF-4) for pH microenvironment analysis in *Pseudomonas aeruginosa* biofilms," *Appl. Environ. Microbiol.* **71**, 2501–2510 (2005).
39. D. G. Davies and G. G. Geesey, "Regulation of the alginate biosynthesis gene algC in Pseudomonas aeruginosa during biofilm development in continuous culture," *Appl. Environ. Microbiol.* **61**, 860–867 (1995).
40. G. J. Tearney, B. E. Bouma, and J. G. Fujimoto, "High-speed phase- and group-delay scanning with a grating-based phase control delay line," *Opt. Lett.* **22**, 1811–1813 (1997).
41. A. L. Oldenburg, J. J. Reynolds, D. L. Marks, and S. A. Boppart, "Fast-Fourier-domain delay line for *in vivo* optical coherence tomography with a polygonal scanner," *Appl. Opt.* **42**, 4606–4611 (2003).
42. A. F. Fercher, C. K. Hitzenberber, G. Kamp, and S. Y. El-Zaiat, "Measurement of intraocular distances by backscattering spectral interferometry," *Opt. Commun.* **117**, 43–48 (1995).
43. J. F. de Boer, B. Cense, B. H. Park, M. C. Pierce, G. J. Tearney, and B. E. Bouma, "Improved signal-to-noise ratio in spectral-domain compared with time-domain optical coherence tomography," *Opt. Lett.* **28**, 2067–2069 (2003).
44. M. A. Choma, M. V. Sarunic, C. Yang, and J. A. Izatt, "Sensitivity advantage of swept source and Fourier-domain optical coherence tomography," *Opt. Express* **11**, 2183–2189 (2003).
45. C. Xi, D. L. Marks, D. S. Parikh, L. Raskin, and S. A. Boppart, "Structural and functional imaging of three-dimensional microfluidic mixers using optical coherence tomography," *Proc. Natl. Acad. Sci. U.S.A.* **101**, 7516–7521 (2004).
46. B. Povazay, K. Bizheva, A. Unterhuber, B. Hermann, H. Sattmann, A. F. Fercher, W. Drexler, A. Apolonski, W. J. Wadsworth, J. C. Knight, P. S. J. Russell, M. Vetterlein, and E. Scherzer, "Submicrometer axial resolution optical coherence tomography," *Opt. Lett.* **27**, 1800–1802 (2002).
47. W. Drexler, U. Morgner, F. X. Kartner, C. Pitris, S. A. Boppart, X. D. Li, E. P. Ippen, and J. G. Fujimoto, "*In vivo* ultrahigh-resolution optical coherence tomography," *Opt. Lett.* **24**, 1221–1223 (1999).
48. X. J. Wang, T. E. Milner, and J. S. Nelson, "Characterization of fluid-flow velocity by optical doppler tomography," *Opt. Lett.* **20**, 1337–1339 (1995).
49. Z. P. Chen, T. E. Milner, D. Dave, and J. S. Nelson, "Optical Doppler tomographic imaging of fluid flow velocity in highly scattering media," *Opt. Lett.* **22**, 64–66 (1997).
50. M. D. Kulkarni, T. G. van Leeuwen, S. Yazdanfar, and J. A. Izatt, "Velocity-estimation accuracy and frame-rate limitations in color Doppler optical coherence tomography," *Opt. Lett.* **23**, 1057–1059 (1998).
51. A. W. Schaefer, J. J. Reynolds, D. L. Marks, and S. A. Boppart, "Real-time digital signal processing-based optical coherence tomography and Doppler optical coherence tomography," *IEEE Trans. Biomed. Eng.* **51**, 186–190 (2004).
52. U. Morgner, W. Drexler, F. X. Kartner, X. D. Li, C. Pitris, E. P. Ippen, and J. G. Fujimoto, "Spectroscopic optical coherence tomography," *Opt. Lett.* **25**, 111–113 (2000).
53. C. Y. Xu, P. S. Carney, and S. A. Boppart, "Wavelength-dependent scattering in spectroscopic optical coherence tomography," *Opt. Express* **13**, 5450–5462 (2005).
54. C. Y. Xu, F. Kamalabadi, and S. A. Boppart, "Comparative performance analysis of time-frequency distributions for spectroscopic optical coherence tomography," *Appl. Opt.* **44**, 1813–1822 (2005).
55. B. E. Bouma, G. J. Tearney, C. C. Compton, and N. S. Nishioka, "High-resolution imaging of the human esophagus and stomach *in vivo* using optical coherence tomography," *Gastrointest Endosc* **51**, 467–474 (2000).
56. X. D. Li, S. A. Boppart, J. Van Dam, H. Mashimo, M. Mutinga, W. Drexler, M. Klein, C. Pitris, M. L. Krinsky, M. E. Brezinski, and J. G. Fujimoto, "Optical coherence tomography: Advanced technology for the endoscopic imaging of Barrett's esophagus," *Endoscopy* **32**, 921–930 (2000).
57. M. V. Sivak, K. Kobayashi, J. A. Izatt, A. M. Rollins, R. Ungrunyawee, A. Chak, R. C. K. Wong, G. A. Isenberg, and J. Willis, "High-resolution endoscopic imaging of the GI tract using optical coherence tomography," *Gastrointest Endosc* **51**, 474–479 (2000).
58. I. K. Jang, G. J. Tearney, B. MacNeill, M. Takano, F. Moselewski, N. Iftima, M. Shishkov, S. Houser, H. T. Aretz, E. F. Halpern, and B. E. Bouma, "*In vivo* characterization of coronary atherosclerotic plaque by use of optical coherence tomography," *Circulation* **111**, 1551–1555 (2005).